Supplemental data

Cloning. Human LRP6 ECD, mouse Fz8 CRD (1-155, [1]) and full-length human Dkk1 cDNA were cloned by PCR amplification from an in-house generated full-length clone using Taq polymerase. Using these cDNAs as templates for subcloning, sets of 4 PCR primers were designed to amplify the domains of interest from LRP6 and Fz8. The primers contained the coding sequences for a C-terminal His_6 tag as well as the nucleotides required for adding portions of the restriction sites BamHI and EcoRI to the resulting PCR products. Denaturation and reannealing of the resulting PCR products produced a population of DNA in which 25% of the products contained the appropriate nucleotides to represent BamHI and EcoRI overhangs at the 5' and 3' ends of the domains of interest, respectively. This DNA mixture was then ligated into a modified pAcGP67 baculovirus DNA transfer vector (BD Pharmingen) for baculovirus generation and extracellular expression in *Sf-9* or T*ni* insect cells (Expression Systems, LLC, Woodland CA.). Dkk1 was introduced by standard cloning techniques into the pVL1393 vector (BD Pharmingen) using Sma1 and BamH1 sites. The integrity of all expression constructs was confirmed by DNA sequencing.

Mass Spectrometry Analysis. 20 µL of full length LRP6 protein at a concentration of 1 mg/ml was deglycosylated with PNGaseF (New England BioLabs, 1:75 ratio), in 50mM Tris-HCl pH 7.5 for 4 h at 45 °C. The deglycosylated protein was then reduced with dithiothreitol (10 mM; 50 °C for 1 h) and alkylated with iodoacetamide (50 mM; room temperature in the dark for 30 min). Excess iodoacetamide was quenched with 3 mM dithiothreitol in the dark at room temperature for 30 min. The sample was then split into two aliquots of 10 µL each. One sample was treated with chymotrypsin (Roche, 1:100 ratio) and the other with Glu-C (Roche, 1:100 ratio). The enzymatically digested samples were analyzed by capillary reverse phase UPLC-ESI MS/MS on a LTQ-Orbitrap XL (ThermoFisher). The samples were acidified and diluted in 0.1% trifluoroacetic acid. 1 µL (108 fmol) of each sample was directly loaded in Buffer A (0.1% trifluoroacetic acid in water) onto a 100 µm x 100 nm, 1.7 µm, BEH130 C18 capillary column (Waters Corp). Peptides were eluted with a 40 min gradient of 5%-90% Buffer B (0.1 % formic acid in 98 % acetonitrile, 2 % water) at 1.00 µl/min generated by an ultra performance LC system (nanoAcquity UPLC, Waters Corp). Eluted peptides were introduced to the mass spectrometer by electrospray ionization through the application of a 2.0 kV potential to the PicoFrit emitter (New Objective) through a liquid junction. Mass spectral data were acquired using a method where one full MS scan in the Orbitrap (375-1600 m/z) was followed by 7 data-dependent scans. For the data dependent-scans, the top 7 most abundant ions were subjected to collision-induced dissociation in the LTQ throughout the LC gradient. In addition to the data-dependent analysis, targeted mass spectral analysis was also performed using methods consisting of one full MS scan (375-1600m/z) in the Orbitrap at a resolution of 60,000 followed by 8 product ion scans (MS^2). For the 8 targeted scan events, each mass was successively subjected to collision-induced dissociation in a cycle repeated in the LTQ throughout the LC gradient. Ions chosen for the various targeted experiments included the doubly and triply charged ions of the deamidated and non-deamidated forms of the enzymatic peptides flanking the 10 potential N-linked glycosylation sites. There were a total of 5 mass spectrometry methods created. In method 1, the targeted ions consisted of 551.31, 367.88, 550.82, and 367.55 m/z corresponding to the peptides flanking N42 enzymatically generated by Glu-C; and 669.36, 668.87, 1017.52, and 1017.03 m/z corresponding to the cleaved and singly miscleaved peptide flanking N81 as produced by the Glu-C enzyme. In method 2, the targeted ions consisted of 1078.00, 719.00, 1077.51, 718.68, 866.49, 578.00, 866.00, and 577.67 m/z corresponding to the peptides flanking N281 and N433 enzymatically generated by Glu-C. In method 3, the targeted ions consisted of 963.03, 642.35, 962.54, 642.03, 919.99, 613.66, 919.50, and 613.33 m/z corresponding to the peptides flanking N486 and N692 of LRP6 as generated by Glu-C enzyme. In method 4, the targeted ions consisted of 1006.02,

671.02, 1005.04, 670.36, 608.83, 406.22, 608.33, and 405.90 m/z corresponding to the peptides flanking N859, N865, and N1039 of LRP6 as generated by Glu-C enzyme. In method 5, the targeted ions consisted of 828.37, 552.91, 827.88, 552.25, 1157.93, 1157.60, 1245.59 and 1245.10 m/z corresponding to the chymotryptic peptides flanking N42, N81, and N926 of LRP6. Tandem mass spectral results were submitted for database searching using the Mascot program (Matrix Science) against both a subset protein database containing the sequence of interest and the Swissprot database with 30 ppm precursor ion mass and 0.8 Da MS/MS tolerance. Deamidated peptide identifications were confirmed by manual interpretation of the mass spectral data.

Cellular β-catenin Assay. On Day 1, mouse L-cells (5000 cells / 20 µL / well) were seeded in a clear bottomed, black-walled 384-well plate and grown for 24 h at 37 °C / 5% CO_2. On Day 2, the cells were treated with 20 µL growth medium containing 2X stock of Wnt3a, Fz8 CRD, LRP6, Dkk1 or combinations of these proteins as indicated, and then incubated for 6 h at 37 °C / 5% CO_2. Cells were then fixed in 4% PFA by adding 20 µl of 12% PFA directly to the wells for 1 h at room temperature. The wells were washed three times with PBS (50 µl/well), permeabilized with PBS / 0.1% Triton X-100 (50 µl/well, three times, 2 min each), and blocked in LI-COR buffer (50 µl/well) for 2 h at room temperature (or, alternatively, overnight at 4 °C). The wells were then incubated with mouse anti-β-catenin antibody (Abcam, 1: 200 for optimal signal-to-noise ratio) in LI-COR blocking buffer for 2 h at room temperature (20 µL/well) and subsequently washed with PBS / 0.1% Tween-20 (50 µL/well, three times). Infrared anti-mouse IRDye800CW secondary antibody (1: 200) and DRAQ5 (1: 10,000) in PBS / 0.5% Tween-20 were then added (20 µL/well). The plates were incubated for 1 h at room temperature, and the wells were washed with PBS / 0.1% Tween-20 (three times) and incubated in PBS (50 µL/well). The plates were covered with black seals and imaged on an Odyssey infrared scanner using microplate2 settings with sensitivity of 5 in both the 700 and 800 nm wavelength channels. Data were acquired by using Odyssey software, exported and analyzed in Excel (Microsoft, Redmond, WA) or KaleidaGraph (Synergy Software). β-catenin values were background-subtracted from wells treated only with secondary antibody, and then normalized to cell numbers by dividing by the total DNA fluorescence signal to account for any fluctuations in cell number.

Supplemental Figure Legends

Figure S1. Insect cell expression and purification of LRP6 and Fz8 extracellular domains. (A) Protein domains and construct sequence boundaries for Fz8 CRD and LRP6 ECD. Molecular weight, number of cysteines and mass spectrometry analysis of each molecule is shown. To analyze the glycosylation status of LRP6 and Fz 8 CRD, they were subjected to PNGaseF treatment followed by mass spectrometry analysis. Fz8 CRD contains one glycosylation site at N49, in agreement with the reported glycosylation for Fz8 CRD isolated from mammalian cells [1]. LRP6 ECD contains four N-linked glycosylation sites at positions 42 of β-propeller one, 433 of β-propeller two, 692 and 865 of β-propeller three. These four residues in LRP6 are strictly conserved in mammals (see Fig. S1E). Therefore, it seems likely that these sites will be glycosylated in mammalian cells, although it is not currently known whether glycosylation plays a role in LRP6 function. (B) Difference in LRP6 protein expression between S*f*9 and T*ni* Pro cells using the wild type or GP67 (baculovirus coat protein) secretion signals. (C) Purity of each fraction during purification of the LRP6 E3E4 protein. Tot = total fraction, FT = flow through, W = wash, Ni = Fraction eluted from the Ni affinity column, GF = pool fraction from gel filtration. (D) SDS-PAGE analysis of purified proteins obtained after gel filtration. Lane 1 = Fz8 CRD, lane 2 = LRP6 E1E2, lane 3 = LRP6 E3E4, lane 4 = LRP6 E3E4 LDL, lane 5 = LRP6 E1E4, lane 6 = LRP6 FL ECD. (E) LRP6 primary sequence alignment. Sequences of LRP6, Hs (Homo Sapiens), Mm (Mus musculus), Gg (Gallus gallus), Xl (Xenopus Laevis), Dr (Danio rerio), Arrow Dm (Drosophila melanogaster) and LRP5 Hs (Homo sapiens) were aligned using an in-house program. Construct boundaries described in Fig S1A are indicated with red squares. Glycosylation sites identified by mass spectrometry are indicated by the blue stars.

Figure S2. Dkk1 competes with Wnt3a for LRP6 binding. Pre-binding of Dkk1 to LRP6 (red trace) inhibits the full binding of Wnt3a to LRP6 (blue trace).

Figure S3. Soluble Fz8 CRD inhibits Wnt3a-mediated β-catenin stabilization by direct binding to Wnt3a. (A) Binding assay between C-terminal Fc-Fusion of Fz8 CRD (coated on the anti-human Fc biosensor) and Wnt3a in solution (K_D = 4 nM). Note: We initially obtained a biotinylated form of Fz8 CRD by co-expressing a C-terminal His_6-Avi-tagged version of Fz8 CRD with biotin ligase in insect cells. Wnt3a binding to this version of Fz8 CRD immobilized on Streptavidin biosensors was not well defined. As a result, Fz8 CRD-Fc fusion was used instead in the binding assays. (B) Fz8 CRD inhibits Wnt3a-mediated β-catenin stabilization with IC_{50} = 0.8 nM. Wnt3a concentration used is 0.6 nM.

Figure S4. Fz8 CRD behaves as a monomeric protein. (A) Comparison of Fz8 CRD gel-filtration profile (blue trace) to a Bio-Rad gel filtration standard (red trace) on a Superdex 200 16/100 column. The major peak for Fz8 CRD has a similar retention time as the 17 kDa standard, suggesting that Fz8 CRD is mainly monomeric. This is in agreement with what is known for Fz8 CRD isolated from CHO cells [1].

Figure S5. LRP6 E1E4 binds to the Wnt3a-Fz8 CRD binary complex. Graph corresponds to a detailed view of the third step (LRP6 binding step) of Figure 3B. The interaction between LRP6 E1E4 and the Fz8/Wnt3a binary complex is dependent on the concentration of E1E4.

Figure S6. Kinetics of Wnt5a and Wnt5b binding to Fz8 CRD. (A) Binding assay between C-terminal Fc-Fusion of Fz8 CRD coated on the anti-Fc biosensor tip and Wnt5a in solution (K_D = 50 nM). (B) Binding assay between C-terminal Fc-Fusion of Fz8 CRD coated on the anti-Fc biosensor tip and Wnt5b in solution (K_D = 37 nM).

Figure S7. Dkk1 competes with Wnt9b for LRP6 binding. (A) Direct binding assay between C-terminal biotinylated LRP6 E1E4 coated on the Streptavidin biosensor and Wnt9b in solution (K_D = 11 nM). (B) Pre-binding of Dkk1 to LRP6 inhibits binding of Wnt9b to LRP6 (red trace). The blue trace is a control for Wnt9b binding to LRP6 in the absence of Dkk1. (C) Detailed view of the third step of the experiment described in (B).

Figure S8. Wnt3a, Wnt9b and Dkk1 binding to LRP6 E1E2 and E3E4. (A) Wnt9b binds to LRP6 E1E2; K_D = 7 nM. (B) Wnt3a binds to LRP6 E3E4; K_D = 174 nM. (C) Dkk1 binds to LRP6 E1E2; K_D = 64 nM. (D) Dkk1 binds to LRP6 E3E4; K_D = 21 nM.

Figure S9. Dkk1 utilizes a common surface to bind to LRP6 E1E2 and E3E4. Pre-binding of Dkk1 to LRP6 E3E4 prevents binding of Dkk1 to E1E2.

1. Dann, C.E. et al. Insights into Wnt binding and signalling from the structures of two Frizzled cysteine-rich domains. *Nature* **412**, 86-90 (2001).

Figure S1, Bourhis et al.

A

	Boundaries	Mw (kDa)	number ofcysteines	Mass spectrometry analysis: Number of peptides	Mass spectrometry analysis: Coverage (%)	Mass spectrometry analysis: Glycosylation
Frizzled 8 CRD	A28-D155	16.1	10	6	46	Yes, Glycosylation at N49
LRP6 FL ECD	M1-T1371	155.5	47	60	55	
LRP6 E1E4	A20-Q1253	140.5	28	61	61	
LRP6 E1E2	A20-E631	70.2	14	27	50	Yes Glycosylation at: N42; N433; N692; N865
LRP6 E3E4	E631-Q1253	71.5	14	32	64	
LRP6 E3E4 LDL	E631-T1371	84.5	31	36	64	

YWTD β-propeller EGF-like domain LDLR type A repeat Cysteine rich domain (CRD)

B

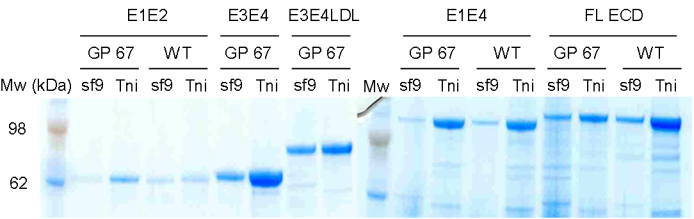

C

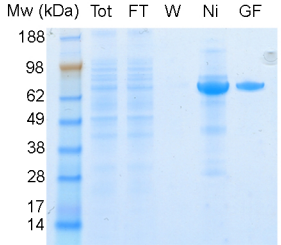

D

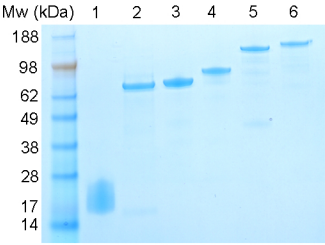

Figure S1E, Bourhis et al.

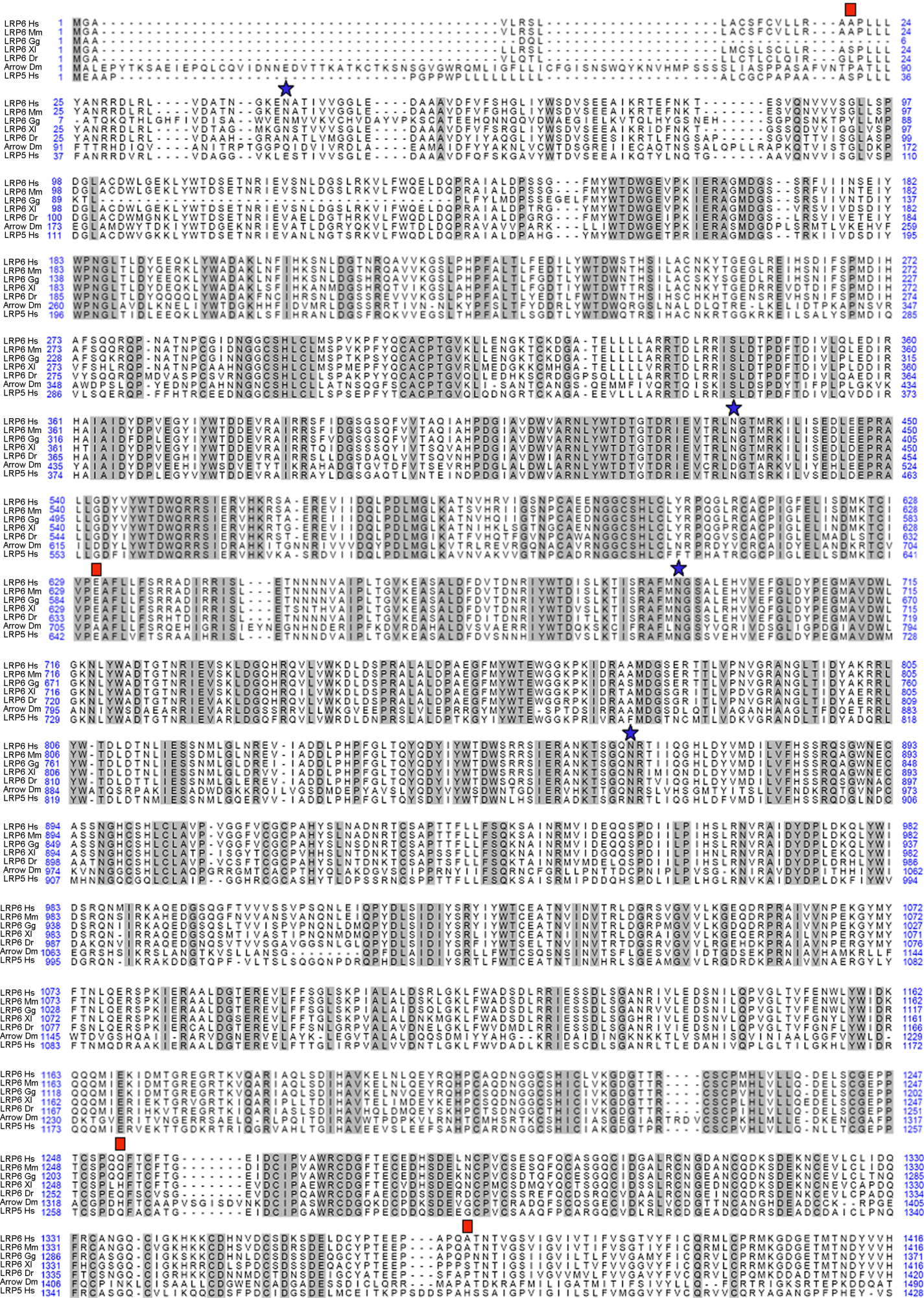

Figure S2, Bourhis et al.

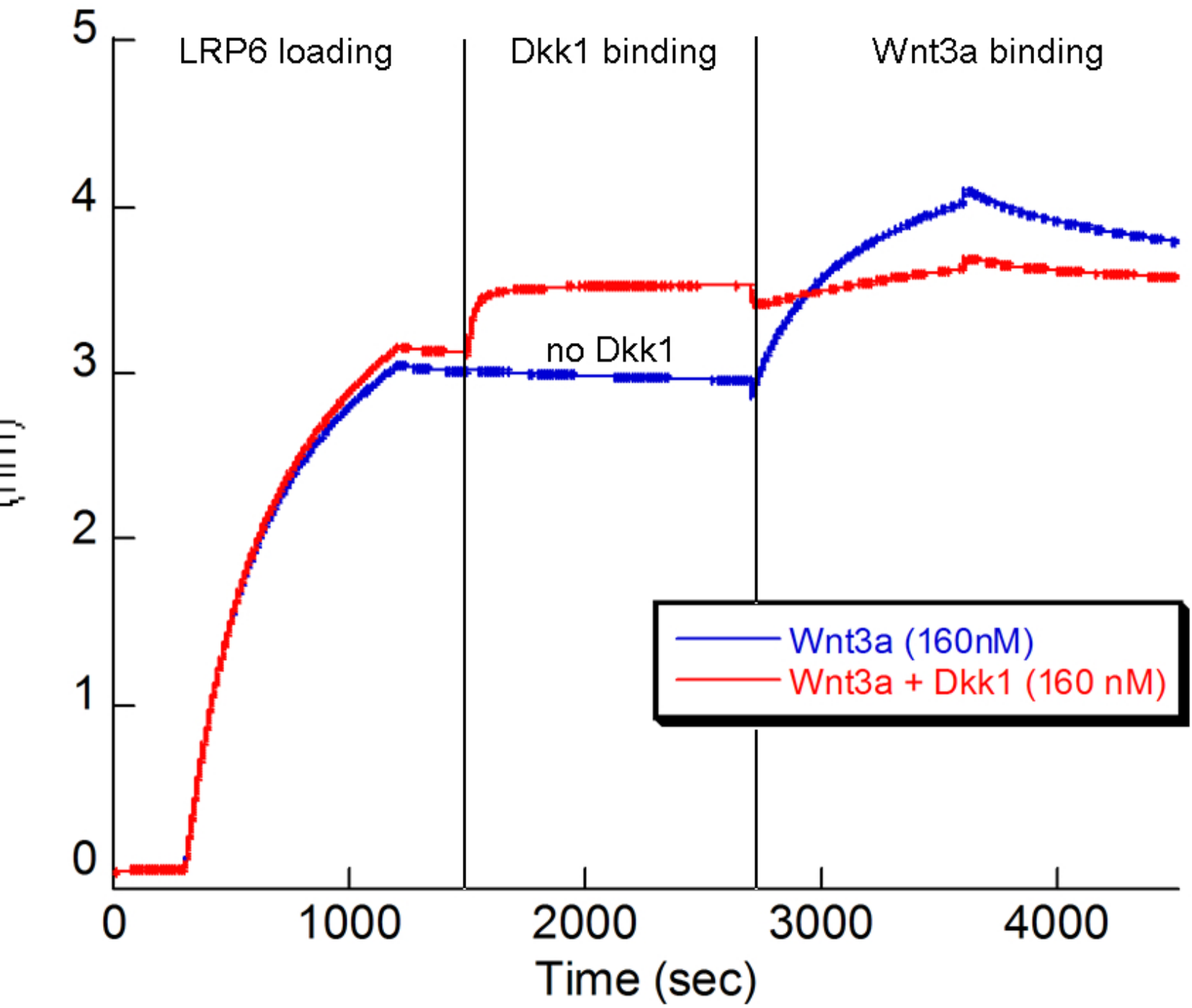

Figure S3, Bourhis et al.

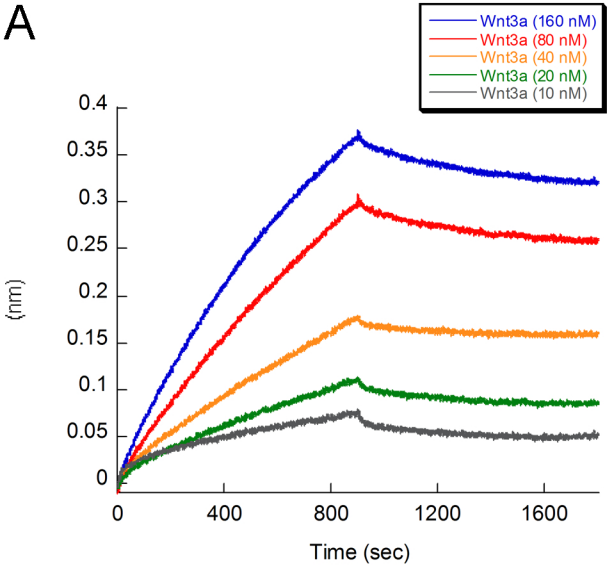

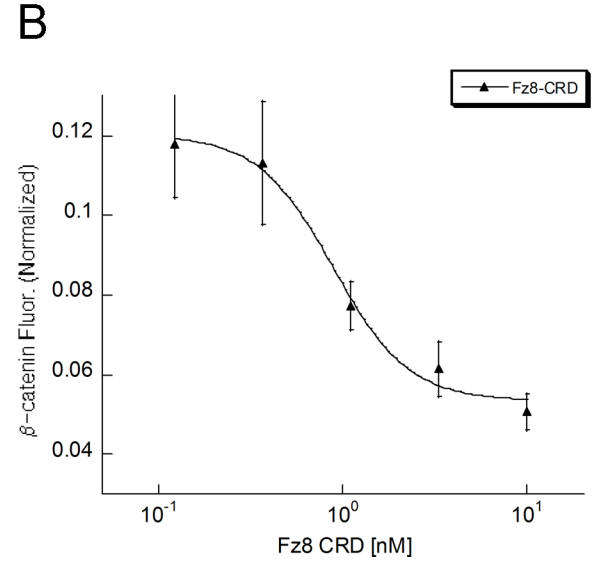

Figure S4, Bourhis et al.

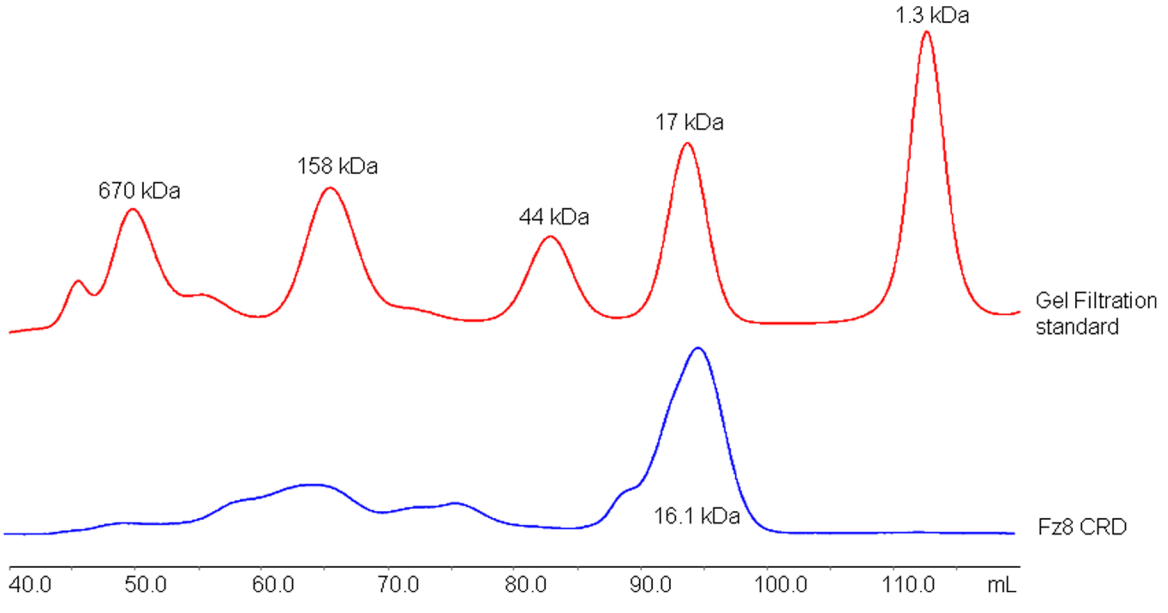

Figure S5, Bourhis et al.

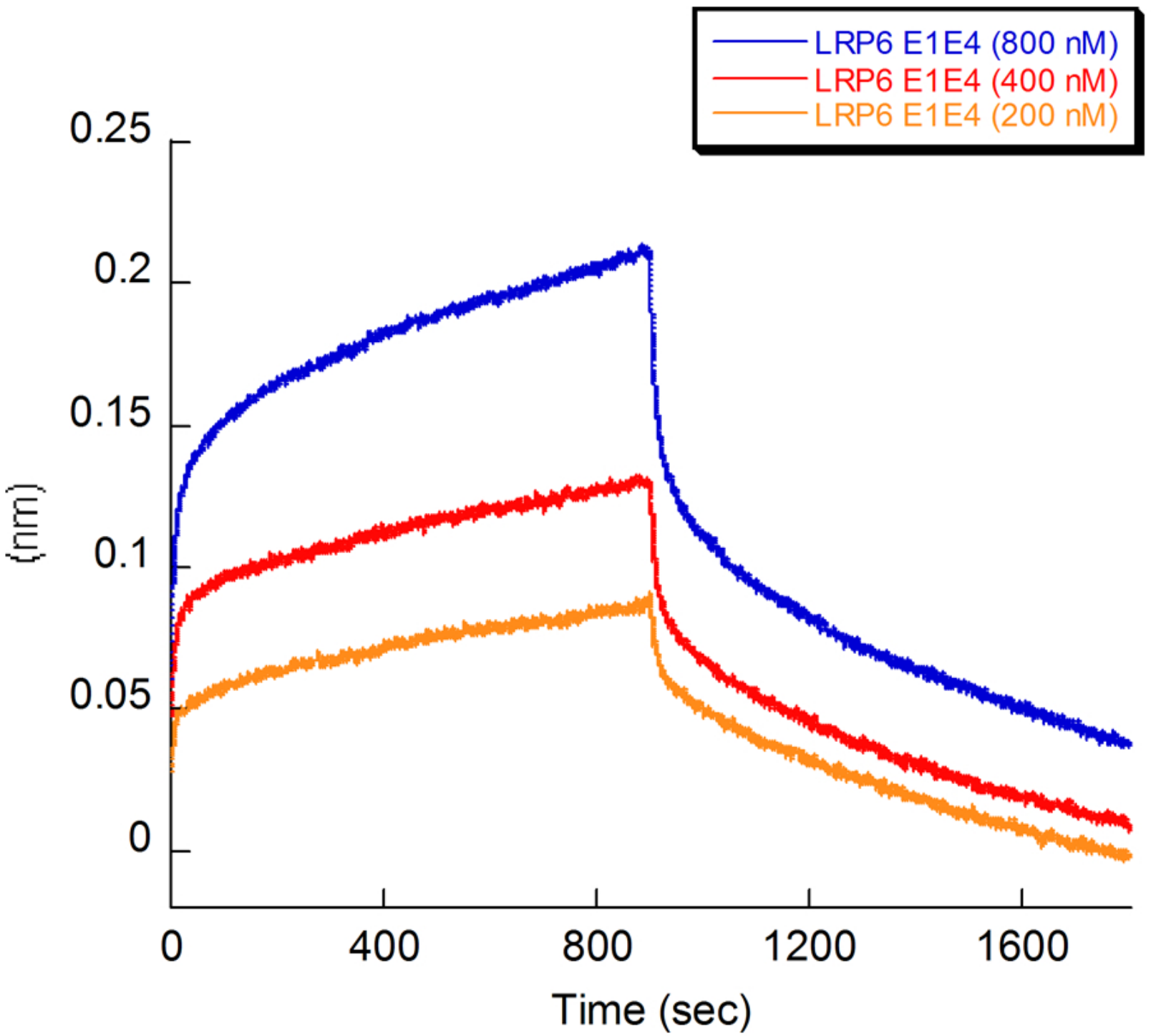

Figure S6, Bourhis et al.

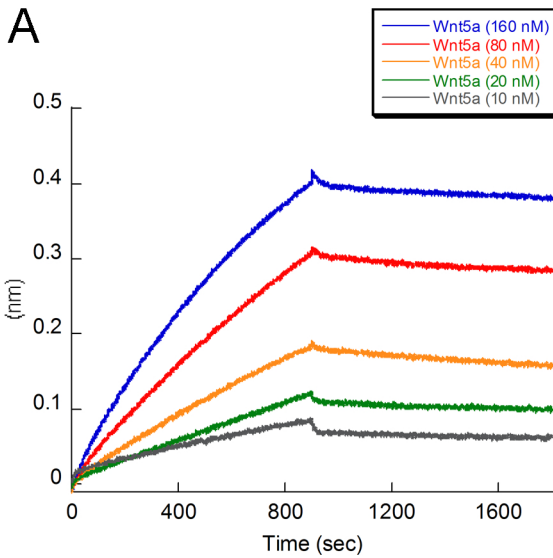

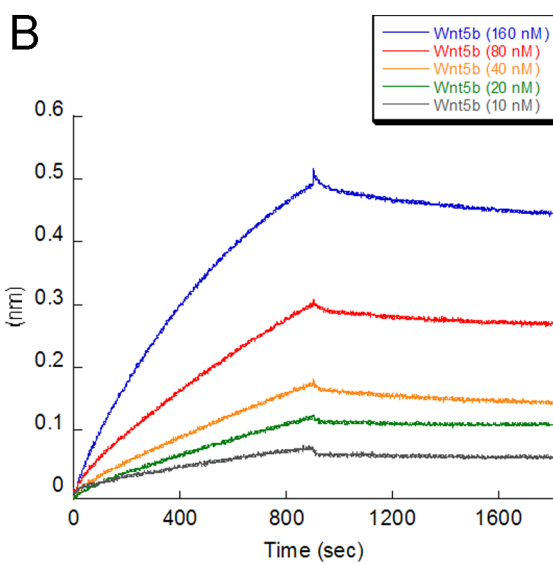

Figure S7, Bourhis et al.

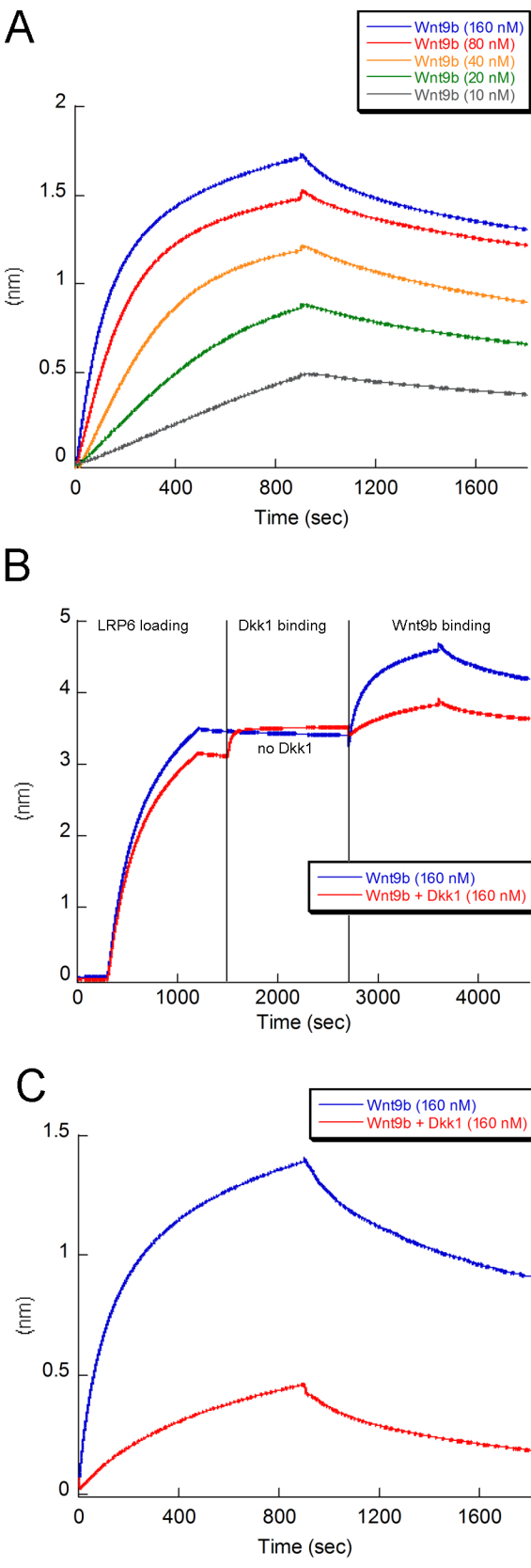

Figure S8, Bourhis et al.

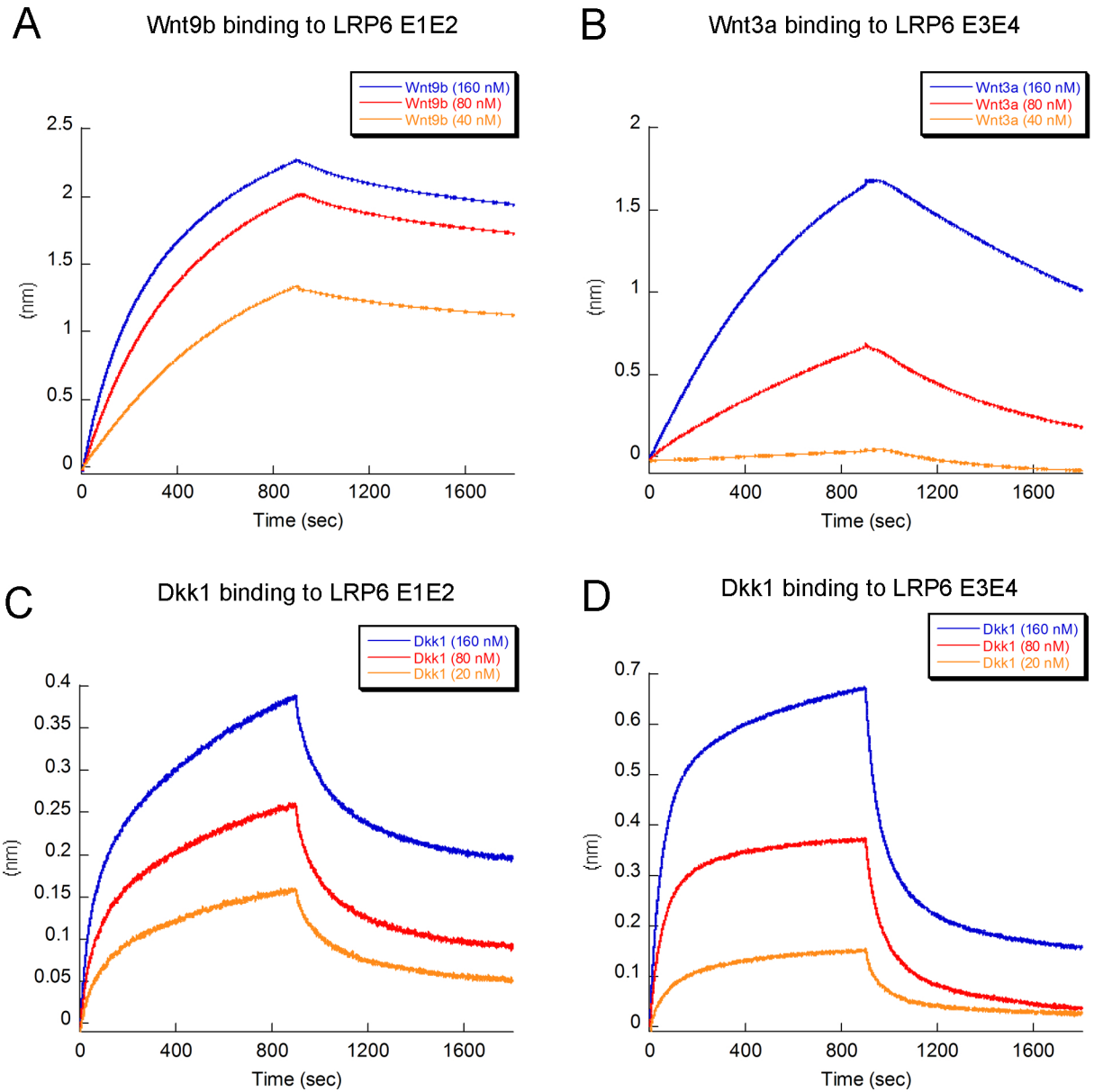

Figure S9, Bourhis et al.